Advanced Open Rotor Noise

M. J. Kingan[1],

[1]Department of Mechanical Engineering, University of Auckland, Auckland, New Zealand

ABSTRACT

A contra-rotating advanced open rotor is a novel aeronautical propulsor which promises significant reductions in fuel burn relative to current generation turbofan engines. It has been the subject of much research by the aeronautical industry over the past decade. This paper briefly summarises a number of experimental investigations which have been undertaken using model-scale rotors and describes some of the issues encountered during, and findings from, these tests. A description of a relatively straightforward 'frequency-domain' analytical method for predicting the tonal noise produced by these engines is also provided. The paper concludes with demonstration of how this analytical method can be used to assist in the design of a quiet contra-rotating open rotor engine.

1. INTRODUCTION

A cut-away schematic of an advanced open rotor engine is shown in figure 1 below. Thrust is produced by the two contra-rotating coaxial 'open rotors' which, for this engine, are driven by a gas turbine housed within a large centerbody which extends both fore and aft of the rotors. The downstream rotor is used to recover the swirl from the wake of the upstream rotor which improves the efficiency relative to a single rotor engine.

It is well-known that the propulsive efficiency of conventional turbofan engines can be improved by increasing the engine diameter and thus the bypass ratio. This approach is limited for turbofan engines by the corresponding increase in drag and weight associated with the nacelle as engine diameter increases. The lack of a shroud or outer nacelle on an open rotor engine means that the diameter of the rotors can be much larger than the fan of an equivalent turbofan engine. This larger diameter achieves the effect of a higher bypass ratio which results in a significant fuel efficiency improvement relative to current generation turbofan engines (Parker (2010)).

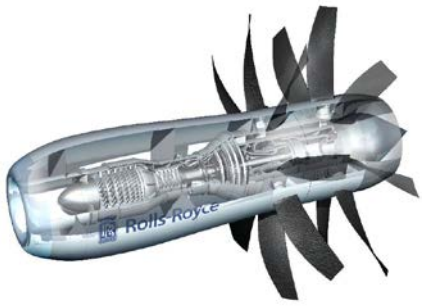

Figure 1: Cut-away schematic of an advanced open rotor (courtesy of Rolls-Royce plc.)

The lack of a nacelle or shroud to shield and attenuate noise generated by the rotor blades means that effort needs to be put into the rotor design to ensure that the level of this noise is acceptably low. This presents some challenges, but model-scale testing and predictions have shown that this should be achievable (Fuss (2011)).

The noise spectrum produced by the open rotor consists of a significant broadband level in addition to a multitude of tones. The tones produced by the rotor blades include the usual 'rotor-alone' tones which occur at integer multiples of the blade passing frequency of each rotor as well as 'interaction' tones produced by the interaction of the rotor blades with the unsteady flow-field from the adjacent rotor. Rotor-alone tones are primarily caused by the steady loading and thickness of the rotor blades. Interaction tones are believed to be primarily produced by the periodic unsteady loading on the rotor blades.

The purpose of this paper is to give a general overview of some of the recent research undertaken on open rotor noise in which the author took part. In section 2 a description of some experiments to measure open rotor noise from model-scale rigs is described. These tests were used to assess noise and aerodynamic performance and

to validate prediction methods. A discussion of some of the issues encountered during these tests and the interesting results which were obtained is included. Section 3 contains a description of a relatively straightforward analytical method for predicting the tones produced by the interaction of the viscous wakes from the upstream rotor with the downstream rotor. Asymptotic theory is then applied to these equations and the resulting expressions are used to show how the 'sweep' of the downstream rotor blades can be used to reduce the level of these tones.

2. EXPERIMENTAL TESTING USING MODEL-SCALE ROTORS

Experimental tests using model-scale open rotor rigs are used to assess aerodynamic and acoustic performance. Testing is undertaken at flow speeds representative of the flight condition which is to be simulated. For assessing the performance of the open rotor at take-off and approach conditions, flow speeds are low-enough to allow testing in a large open-jet wind tunnel, which is also convenient for making acoustic measurements. For experiments simulating cruise flight speeds, testing must be undertaken in a transonic wind tunnel, which has a relatively small cross-sectional area and which presents a challenging environment in which to make meaningful acoustic measurements.

2.1 Low-speed testing

Figure 2 below shows a photograph of Rolls-Royce's 'Rig 145' 1/6th scale open rotor rig (with a ~710mm diameter front rotor) installed in the open jet test section of the Large, Low-Speed facility of the German-Dutch Wind tunnels (DNW). Rig 145 was a refurbished version of an earlier 1/5th model-scale open rotor rig known as 'Rig 140' which is described in detail in Kirker (1989). The photograph shown in figure 2 was taken during an experimental campaign conducted in 2008 as part of the European DREAM programme. These tests investigated the effect of various parameters on rotor aerodynamic performance and noise including thrust, blade pitch and tip speed. Note that the rig had two independent motors which allowed testing to be conducted at many different rotor speed ratios. Testing was conducted using an isolated rig and then, in collaboration with Airbus, installed configurations with a pylon upstream of the open rotor were tested.

Figure 2: Testing of a 1/6th scale open rotor rig in the DNW wind tunnel with pylon installed upstream. Picture taken from Parry et al. (2011)

Noise measurements were made during the 2008 test campaign using microphones located outside the open jet. These measurements were affected by the shear layer in two ways. First, sound propagating through the shear layer is refracted which alters the direction of sound propagation. As the noise produced by an open rotor is quite directional, this effect must be quantified if noise data is to be used for assessment purposes. The second effect is commonly referred to as "haystacking" where the energy in the sound at a particular frequency propagating through the shear layer is scattered into adjacent frequencies by turbulence. Haystacking has the effect of broadening and reducing the amplitude of tones produced by the open rotor rig at measurement positions outside

the open jet. The effect becomes more pronounced as frequency increases such that at higher frequencies it can become difficult to identify tones at all.

A second experimental campaign using Rig 145 was undertaken in 2010. These tests used new blades which had been designed using an aeroacoustic optimisation process. In order to overcome the issues encountered in the first set of tests, acoustic measurements were also made using an array of inflow microphones which could be traversed fore and aft of the rig. A photograph of Rig 145 installed in the wind tunnel with the inflow microphone array adjacent is shown in figure 3 below. The microphones were fitted with nose cones in order to minimise the 'pseudo-noise' produced by the turbulent flow over them. Unfortunately, the data at high frequencies measured by these microphones appeared to be affected by a flow resonance within the nose cone. This limited the frequency range of the data collected from these microphones. Note that subsequent experimental test campaigns led by Airbus have used a custom noise measurement system in which microphones were mounted within a traversing aerofoil (see Paquet et al. (2014)).

Figure 3: Testing of a 1/6th scale open rotor rig in the DNW wind tunnel with inflow microphone array. Picture taken from Parry et al. (2011)

The narrow-band and one-third octave band sound pressure spectra measured at a particular observer location using a microphone on the in-flow traverser during the 2010 Rig 145 test campaign is shown in figure 4 below. A narrow-band broadband level was calculated by fitting a moving median curve through the narrow-band data. One-third octave band levels were then separately calculated from the narrowband data for the broadband and tonal noise components of the spectrum. These levels show that, on a one-third octave band basis, the broadband noise levels produced by the aeroacoustically optimised open rotor make an important contribution to the overall noise level. This prompted a significant effort to develop models for the broadband noise produced by the rotor e.g. the methods published in Kingan (2013) and Blandeau et al. (2013). Although many models have been developed or improved for rotor broadband noise more work needs to be done in order to predict all sources of broadband noise accurately.

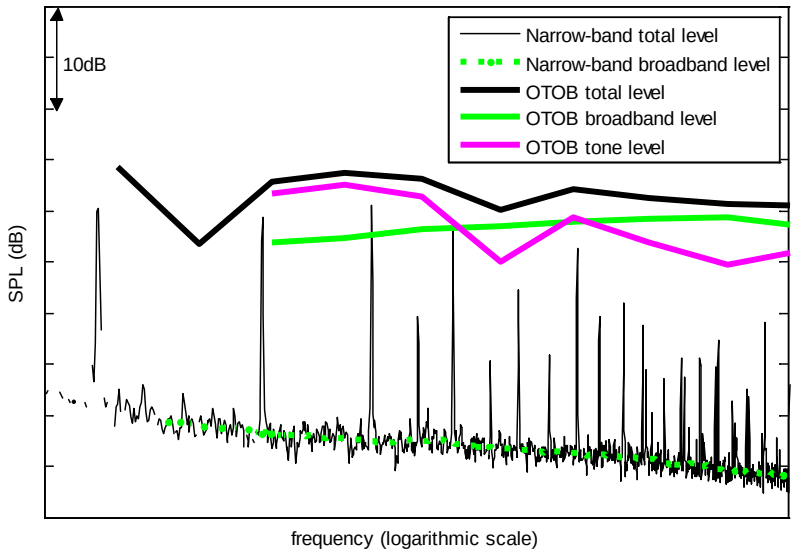

Figure 4: Narrowband and 1/3 octave band SPL produced by an open rotor. From Kingan (2014)

2.2 High-speed testing

Figure 5 below shows a photograph of Rig 145 installed in the transonic wind tunnel located at the Aircraft Research Association (ARA) in Bedford, UK. The rails in the foreground of the photograph are instrumented with an array of microphones which were used to collect noise data at a number of fixed locations. The test section of the wind tunnel was lined with an acoustic liner, the purpose of which was to minimise reverberation within the test section. The rig was tested at a range of flow Mach numbers from 0.2 to 0.8 and at a range of thrusts and front and rear propeller tip speeds. Note that two experimental campaigns were undertaken in the ARA tunnel using Rig 145. These both occurred shortly after corresponding tests using the rig at the DNW open jet facility.

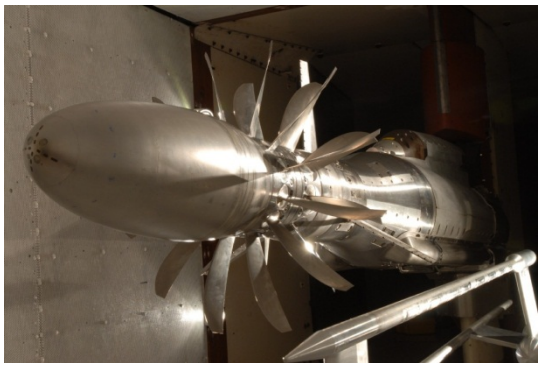

Figure 5: Rolls-Royce's 1/6th scale open rotor rig installed in the ARA wind tunnel in Bedford, UK. Picture courtesy of Rolls-Royce plc.

The effectiveness of the acoustic liner in the wind tunnel test section was found to be reduced at Mach numbers greater than approximately 0.6. When the liner becomes ineffective then reverberation effects can contaminate noise measurements made inside the tunnel. Sureshkumar et al. (2016) have developed a number of models for predicting the noise produced by an open rotor installed within a wind tunnel which have been used to assess the effect of reverberation. They show that measurements taken in the 'near-field' of the propeller close to the rotor tips are least affected by reverberation. This is particularly true of rotor-alone tones for which the acoustic field decays evanescently away from the rotor in the near-field.

Because measurements must be made in very close proximity to the rotor blades when testing in a closed-section wind tunnel, methods for projecting the acoustic data from one location to another (e.g. from the evanescent near field to the acoustic far-field) must be employed. The method of Peake and Boyd (1993) is one

such method which can be used for this purpose. This method works by assuming that the noise field produced by a rotor can be approximated by a rotating point force located at the radius at which the rotor noise sources make the most important contribution to the rotor noise field. The point force is aligned parallel to the local lift force acting on the rotor blade i.e. it is assumed that lift forces are the dominant 'noise source'. Figure 6 below shows the location of the microphone rails relative to the open rotor rig whilst figure 7 shows the levels measured at two of the three microphone rails for a particular rotor-alone tone and also the 'projected level' calculated by projecting the measured level from one rail to the other using the method of Peake and Boyd. The agreement between the projected and measured levels is reasonable.

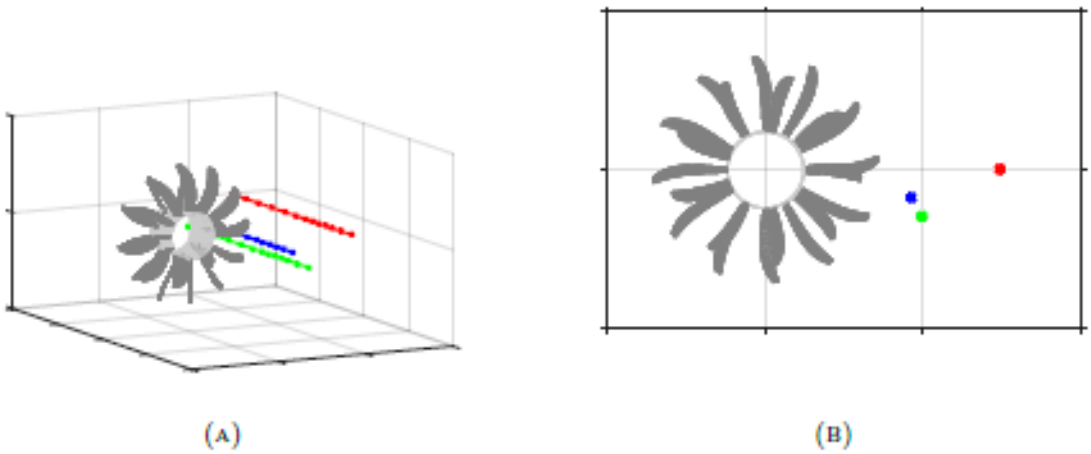

Figure 6: Schematic showing the position of the microphone rails relative to the open rotor during testing at the ARA transonic wind tunnel.

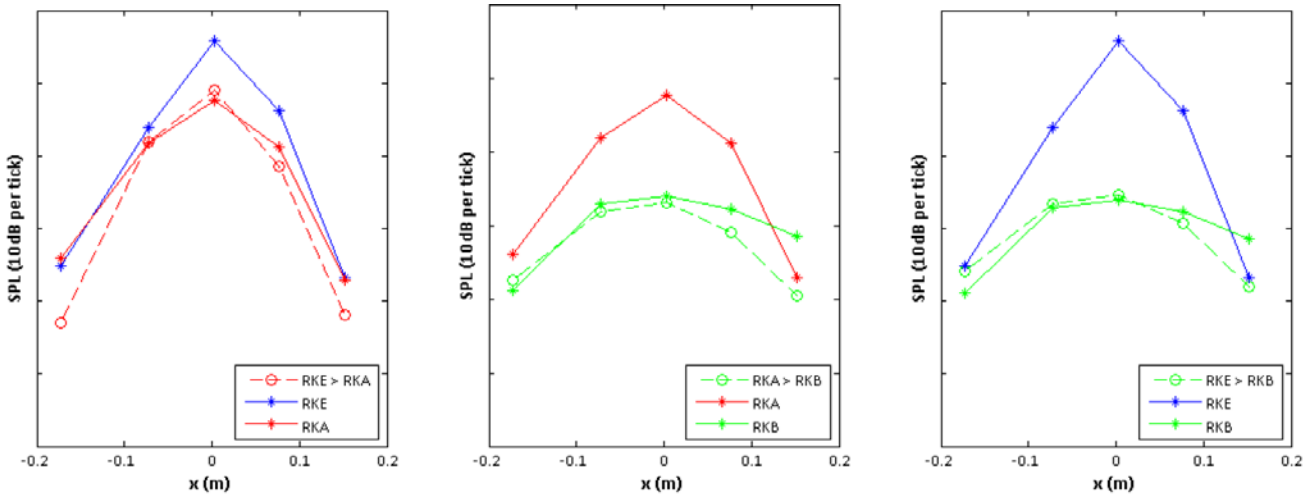

Figure 7: Measured and projected sound pressure levels for a rotor-alone tone during testing at the ARA transonic wind tunnel. Each plot shows measurements taken using microphones on two rails. Measurements at one rail are projected to give the expected level at the other rail.

The projection method can be used to take wind tunnel data, which is measured in the acoustic near-field, and project it to other locations. For example, the measured data could be projected to a sideline location corresponding to the outer surface of the fuselage which would be useful information for estimating the in-cabin noise levels during cruise. Projections could also be made to the acoustic far-field for the purposes of estimating en-route 'community noise levels' produced by an open rotor powered aircraft. Such an approach was adopted in the European project NINHA in which the community noise levels produced by an open rotor powered aircraft during cruise were estimated. Acoustic data from wind tunnel testing using rig 145 was projected from the near-field measurement position to the acoustic far-field and was corrected for scale and atmospheric effects to give a full-

scale far-field noise level for the rotor. The propagation of this sound from the aircraft to the ground was calculated using a ray-tracing algorithm which accounted for the absorption and refraction of sound through the atmosphere. This work indicated that the maximum noise level produced by an open rotor powered aircraft would be equivalent to that of today's turboprop powered aircraft (van Oosten (2014)).

3. ANALYTICAL NOISE PREDICTION OF INTERACTION TONE NOISE

A number of methods for predicting open rotor noise are available and a summary of these can be found in the review paper by the author (Kingan (2014)) which the reader is referred to for further details. As one might expect these methods involve varying degrees of complexity and computational time and range from high fidelity (but time intensive) CFD methods to simple (but quick) analytical methods. The remainder of this paper will be devoted to describing an analytical method for predicting the dominant source of interaction tone noise. The model will then be used to design a quiet open rotor.

For the purposes of analytical modelling, the unsteady flow-field produced by each rotor blade can be decomposed into (1) the viscous wake, (2) the tip-vortex, and (3) the bound potential field. The velocity perturbation associated with each of these fields can then be decomposed into a Fourier series of 'harmonic convected gusts' by making use of the periodicity of the problem in the azimuthal coordinate (the angle through which the blade rotates). The unsteady loading on or 'response' of the adjacent rotor's blades to the each of these gusts is then calculated using well-known 'blade response functions'. Analytical models for the viscous wake and bound potential field sources are described in Parry (1988) whilst a number of models are available for predicting the unsteady field produced by the tip vortex e.g. Roger et al.(2012). The far-field noise radiation can be predicted from the calculated unsteady loading using the analytic 'frequency domain' expressions of Hanson (1985) or Parry (1988).

3.1 Analytic method for predicting viscous wake interaction tones

In this section we develop a model for calculating the tonal noise produced by the unsteady loading on the downstream rotor blades due to their interaction with the viscous wakes of the upstream rotor. This model is a simple extension of the model developed by Parry (1988). For the analysis presented in this paper, it will be convenient to introduce a cylindrical coordinate system, $\{x, r, \phi\}$, where x is the axial coordinate which is collinear with the propeller axis, r is the radial coordinate and ϕ is the azimuthal angle. This coordinate system is shown in figure 8 below. The rotors are immersed in a uniform airflow with Mach number M_x in the negative x-direction relative to the advanced open rotor and the air has ambient density ρ_0 and speed of sound c_0. The upstream and downstream rotors rotate in the negative and positive ϕ-directions at rotational speeds Ω_1 and Ω_2 respectively. The pitch-change axis of the reference blades on the front and rear rotors are located at $\phi = 0$ rad at time $\tau = 0$ s and are separated by a distance g in the axial direction. Also note that the convention adopted in this paper will be that the subscripts 1 and 2 denote parameters associated with the front and rear rotors. The blades of both rotors have chord $c(r)$, sweep $s(r)$, lean $l(r)$ and sectional drag coefficient $C_D(r)$ and both rotors have B blades and have an equal diameter which is denoted D.

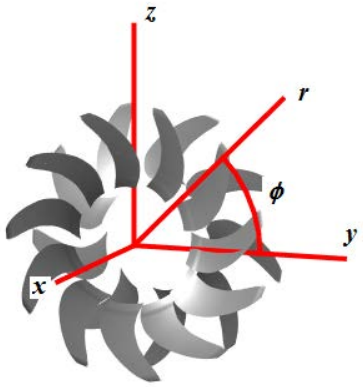

Figure 8: Schematic showing an advanced open rotor and the cylindrical coordinate system

The unsteady loading on the downstream rotor blades at a given radial location is calculated using an equivalent 2D problem where the wakes from an upstream cascade of blades interacts with the blades of a downstream cascade. This situation is illustrated in Figure 9 below. The formulation presented here will make use of a Cartesian coordinate system $\{x, y\}$, where x is an axial coordinate defined such that the airflow has Mach number M_x in the positive x-direction and y is a tangential coordinate which is parallel to the direction in which the blade rows translate. The upstream and downstream blades translate in the negative and positive y-directions at Mach numbers $\Omega_1 r/_0$ and $\Omega_2 r/c_0$ respectively. At time $\tau = 0$ s the pitch-change axis of the front rotor reference blade is aligned with the pitch change axis of the rear rotor reference blade at $y/D = 0$ and the spacing between the mid-chord positions of the blades on each cascade in the y-direction is equal to $2\pi r/B$. The blades are modelled as infinitely thin flat-plates which are aligned with the local flow direction but otherwise have identical characteristics (such as chord-length, sweep, lean and drag coefficient) to the actual rotor blade at that particular radius. Also, the effect of the flow induced by the rotors is neglected such that the stagger angle, α, of each blade is defined by $\tan\alpha = zM_T/M_x$, where $z = 2r/D$ and $M_T = \Omega D/2c_0$.

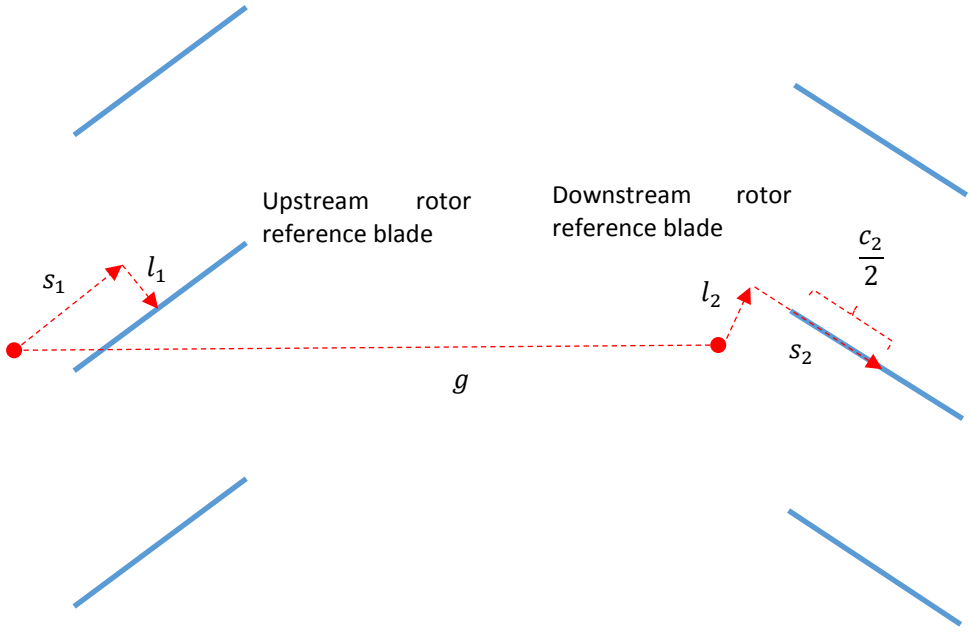

Figure 9: Schematic of the equivalent 2D cascade problem.

In order to describe the development of the wakes from the upstream cascade it is convenient to introduce two coordinate systems which are locked to the upstream blade row and have origins located at the mid-chord of the upstream reference blade. The $\{x_1, y_1\}$ coordinate system has coordinates which a parallel to the global $\{x, y\}$ coordinate system. The $\{X_1, Y_1\}$ coordinate system has coordinates parallel to the chordwise and chord-normal directions and is related to the $\{x_1, y_1\}$ coordinate system by the equations below.

$$X_1 = x_1 \cos\alpha_1 + y_1 \sin\alpha_1, \tag{1}$$

$$Y_1 = -x_1 \sin\alpha_1 + y_1 \cos\alpha_1, \tag{2}$$

The reference blade of the upstream blade row produces a wake with mean deficit velocity u' aligned with the negative X_1-direction at the axial location of the leading edge of the downstream rotor which will be modelled using the 'Schlichting' wake profile

$$u' = U_{r_1} \frac{\sqrt{10}}{18\beta} \left(\frac{c_1 C_{D_1}}{L_1}\right)^{\frac{1}{2}} \left[1 - \left(\frac{Y_1}{b}\right)^{1.5}\right]^2, |Y_1| \leq b \tag{3}$$

where $\beta = 2^{\frac{1}{3}} / \left[4\sqrt{10}\left(\sqrt{2}-1\right)^{2/3}\right]$, U_{r_1} is the velocity of the air relative to the blade and L_1 is the length of the wake which is defined as the distance in the X_1-direction between the mid-chord of the reference blade and the axial location of the point of interest, $b = 4\sqrt{10}\beta b_{1/2}$ and $b_{1/2}$ is defined as $b_{1/2} = \frac{1}{4}\sqrt{C_{D_1} c_1 L_1}$. Substituting eq. (2) into eq. (3) gives an expression for the wake deficit velocity produced by the front rotor reference blade in the $\{x_1, y_1\}$ coordinate system.

In order to calculate the unsteady loading on the downstream blade row, it is necessary to express the front rotor wake velocity deficit in a coordinate system fixed to the rear rotor blades. For this purpose we introduce a blade locked axial/tangential coordinate system $\{x_2, y_2\}$ which is parallel to the axial and tangential coordinates and has its origin located at the leading edge of the reference blade on the downstream blade row. The $\{x_2, y_2\}$ coordinate systems are related to the $\{x_1, y_1\}$ coordinate system by eqs. (4) and (5) below.

$$x_1 = x_2 + g - s_1 \cos\alpha_1 + \left(s_2 - \frac{c_2}{2}\right)\cos\alpha_2 - l_1 \sin\alpha_1 + l_2 \sin\alpha_2, \tag{4}$$

$$y_1 = y_2 + (\Omega_1 + \Omega_2) r\tau + l_1 \cos\alpha_1 - s_1 \sin\alpha_1 - \left(s_2 - \frac{c_2}{2}\right)\sin\alpha_2 + l_2 \cos\alpha_2, \tag{5}$$

It will also be assumed that the downstream rotor is located sufficiently far downstream of the upstream rotor that the wake development (increase in wake width and decrease in the wake centreline velocity deficit) in the axial direction can be neglected in the vicinity of the downstream rotor. Thus we set L_1 equal to its value at the leading edge of the downstream rotor blades.

The mean velocity deficit produced by the upstream blade row, v', is assumed to be equal to the sum of the velocity deficit produced by all the blades on the upstream cascade (which are evenly spaced and identical) which, making use of Poisson's summation theorem can be written as

$$v' = \sum_{n_1=-\infty}^{\infty} \frac{B_1 C_{D_1} c_1 U_{r_1}}{4\pi r \cos\alpha_1} G(k_b) \exp\left\{ i \frac{n_1 B_1}{r} y_1 - i \frac{n_1 B_1}{r} x_1 \tan\alpha_1 \right\}, \tag{6}$$

where

$$k_b = \frac{n_1 B_1 b}{r \cos\alpha_1}, \tag{7}$$

and

$$G(k_b) = \frac{40}{3k_b^4}\left\{ (1 - \cos k_b - k_b \sin k_b) + \frac{k_b^2}{2}\left(\frac{\pi}{2k_b}\right)^{0.5} C\left[\left(\frac{2k_b}{\pi}\right)^{0.5}\right] \right\}, \tag{8}$$

where $C[\ \ ]$ is the Fresnel cosine integral.

One final coordinate transformation is required in order to express the upstream rotor wake velocity deficit incident onto the reference blade of the downstream blade row in a chordwise/chordnormal coordinate system, $\{X_2, Y_2\}$, which is defined by eqs. (9) and (10) below.

$$x_2 = X_2 \cos\alpha_2 + Y_2 \sin\alpha_2, \tag{9}$$

$$y_2 = -X_2 \sin\alpha_2 + Y_2 \cos\alpha_2. \tag{10}$$

Substituting eqs. (9) and (10) into eqs. (7) and (8) and then substituting the resulting expressions into eq. (4) gives

$$v' = \sum_{n_1=-\infty}^{\infty} \frac{B_1 C_{D_1} c_1 U_{r_1}}{4\pi r \cos\alpha_1} G(k_b) \exp\{i n_1 B_1 (\Omega_1 + \Omega_2)\tau\}$$

$$\times \exp\left\{-\mathrm{i}k_X X_2 - \mathrm{i}k_Y Y_2 - \mathrm{i}k_X\left(s_2 - \frac{c_2}{2}\right) - \mathrm{i}k_Y l_2 - \mathrm{i}k_{Y_1}(g\sin\alpha_1 - l_1)\right\}, \tag{11}$$

where

$$k_X = \frac{2n_1B_1}{DM_{r_2}}\left[M_{T_1} + M_{T_2}\right], \tag{12}$$

$$k_Y = -\frac{2n_1B_1}{DM_{r_2}}\left[\frac{M_x}{z} - z\frac{M_{T_1}M_{T_2}}{M_x}\right], \tag{13}$$

and

$$k_{Y_1} = \frac{2n_1B_1M_{r_1}}{zDM_x}. \tag{14}$$

Note that the upstream rotor wake deficit velocity is aligned with the $-X_1$ direction and therefore the upwash velocity (which is the component of velocity in the Y_2 direction) onto the downstream reference blade is given by

$$w = -\sin(\alpha_1 + \alpha_2)\, v'. \tag{15}$$

We therefore have the following expression for the upwash on the chordline of the reference blade of the downstream blade row (on which $Y_2 = 0$)

$$w = \sum_{n_1=-\infty}^{\infty} w_{n_1} \exp\left\{\mathrm{i}k_X\left(U_{r_2}\tau - X_2\right) - \mathrm{i}k_Y Y_2\right\}, \tag{16}$$

where U_{r_2} is the velocity of the downstream blade relative to the air and

$$w_{n_1} = -\sin(\alpha_1 + \alpha_2)\frac{B_1C_{D_1}c_1U_{r_1}}{4\pi r\cos\alpha_1}G(k_b)\exp\left\{-\mathrm{i}k_X\left(s_2 - \frac{c_2}{2}\right) - \mathrm{i}k_Y l_2 - \mathrm{i}k_{Y_1}(g\sin\alpha_1 - l_1)\right\}. \tag{17}$$

The total unsteady lift force per unit area acting on the chordline of the reference blade in the $-Y_2$ direction can be expressed as the sum of the unsteady lift on the blade due to its interaction with each upwash harmonic i.e.

$$\Delta p = \sum_{n_1=-\infty}^{\infty} \Delta p_{n_1} \exp\{\mathrm{i}n_1B_1(\Omega_1 + \Omega_2)\tau\}, \tag{18}$$

where $\Delta p_{n_1}\exp\{\mathrm{i}n_1B_1(\Omega_1 + \Omega_2)\tau\}$ is the response of the reference blade to a gust of the form $w_{n_1}\exp\left\{\mathrm{i}k_X\left(U_{r_2}t - X_2\right) - \mathrm{i}k_Y Y_2\right\}$ and Δp_{n_1} is given by (see, for example, Goldstein (1976)).

$$\Delta p_{n_1} = \frac{2\rho_0U_{r_2}w_{n_1}}{\left[\pi\sigma_2\left(1+M_{r_2}\right)\bar{X}_2\right]^{0.5}}\exp\left\{-\mathrm{i}\frac{\pi}{4} - \mathrm{i}\frac{\sigma_2M_{r_2}}{1+M_{r_2}}\bar{X}_2\right\},\ n_1 \neq 0 \tag{19}$$

where $M_{r_2} = U_{r_2}/c_0$ is the Mach number of the airflow relative to the downstream rotor blade, $\bar{X}_2 = 2X_2/c_2$ is a dimensionless chordwise coordinate and $\sigma_2 = k_Xc_2/2$ is the reduced frequency of the gust harmonic interacting with the rear rotor blade. We do not consider the $n_1 = 0$ terms in the analysis presented here as these correspond to the steady component of loading on the rotor blades.

Following the derivation presented by Hanson (1985), the far-field tonal sound pressure produced by the periodic lift forces on the downstream rotor of a contra-rotating open rotor due to the wakes shed by the upstream rotor is given by the following expression

$$p = \frac{\mathrm{i}\rho_0c_0^2B_2D}{8\pi R_e(1-M_x\cos\theta_e)}\sum_{n_1=-\infty}^{\infty}\sum_{n_2=-\infty}^{\infty}\exp\left\{\mathrm{i}\omega\left(t - \frac{R_e}{c_0}\right) - \mathrm{i}\nu\left(\phi - \frac{\pi}{2}\right)\right\}I_{n_1,n_2}, \tag{20}$$

where

$$I_{n_1,n_2} = \int_{z_h}^{1} M_{r_2}^2 \exp\{-\mathrm{i}(\phi_l + \phi_s)\} J_\nu\left(\frac{\nu}{z^*} z\right) k_y \frac{C_{Ln_1}}{2} \psi_{L_{n_1}}(k_x)\, dz, \tag{21}$$

$$\omega = n_1 B_1 \Omega_1 + n_2 B_2 \Omega_2, \tag{22}$$

$$\nu = n_2 B_2 - n_1 B_1, \tag{23}$$

$$k_x = \frac{2}{M_{r_2}}\left[\frac{(n_1 B_1 M_{T_1} + n_2 B_2 M_{T_2}) M_x \cos\theta_e}{(1 - M_x \cos\theta_e)} + \nu M_{T_2}\right]\frac{c_2}{D}, \tag{24}$$

$$k_y = -\frac{2}{M_{r_2}}\left[\frac{(n_1 B_1 M_{T_1} + n_2 B_2 M_{T_2}) M_{T_2} z \cos\theta_e}{(1 - M_x \cos\theta_e)} - \nu \frac{M_x}{z}\right]\frac{c_2}{D}, \tag{25}$$

$$\phi_s = \frac{2}{M_{r_2}}\left[\frac{(n_1 B_1 M_{T_1} + n_2 B_2 M_{T_2}) M_x \cos\theta_e}{(1 - M_x \cos\theta_e)} + \nu M_{T_2}\right]\frac{s_2}{D}, \tag{26}$$

$$\phi_l = \frac{2}{M_{r_2}}\left[\frac{(n_1 B_1 M_{T_1} + n_2 B_2 M_{T_2}) M_{T_2} z \cos\theta_e}{(1 - M_x \cos\theta_e)} - \nu \frac{M_x}{z}\right]\frac{l_2}{D}, \tag{27}$$

$$z^* = \frac{(1 - M_x \cos\theta_e)\nu}{(n_1 B_1 M_{T_1} + n_2 B_2 M_{T_2}) \sin\theta_e}, \tag{28}$$

and

$$\frac{1}{2}\rho_0 U_{r_2}^2 c_2 C_{Ln_1} \psi_{Ln_1}(k_x) = \int_0^{c_2} \Delta p_{n_1} \exp\left\{-\mathrm{i}\frac{k_x}{2}\left(\frac{2X_2}{c_2} - 1\right)\right\} \mathrm{d}X_2, \tag{29}$$

where Δp_{n_1} is the n_1^{th} Fourier harmonic of the unsteady pressure jump on the downstream blade row.

The value z^*, defined in eq. (28) is an important parameter; it represents the point at which the argument of the Bessel function becomes equal to its order and, significantly, is close to the point at which the Bessel function achieves its maximum value.

Substituting eq. (19) into eq. (29) and evaluating the integral yields for $n_1 \neq 0$

$$C_{Ln_1}\psi_{Ln_1}(k_x) = \frac{w_{n_1}}{U_{r_2}} \frac{2\sqrt{2}\exp\left\{\mathrm{i}\frac{k_x}{2} - \mathrm{i}\frac{\pi}{4}\right\}}{\sigma_2^{0.5}\left(1 + M_{r_2}\right)^{0.5}\left[\frac{\sigma_2 M_{r_2}}{(1+M_{r_2})} + \frac{k_x}{2}\right]^{0.5}} E^*\left(\frac{2}{\sqrt{\pi}}\left[\frac{\sigma_2 M_{r_2}}{(1+M_{r_2})} + \frac{k_x}{2}\right]^{0.5}\right), \tag{30}$$

where E^* is the conjugate of the complex Fresnel integral.

Having described the full equations for the unsteady response of the downstream blade row to the front rotor wakes, and the resultant sound radiation to the far-field, we turn to asymptotic analysis of the formulae to aid interpretation of the underlying physics.

We start by noticing that the Bessel function in eq. (21) originates from an integration of the noise sources over the propeller disc and we can return to the original form by replacing it with Bessel's integral

$$J_\nu\left(\frac{\nu}{z^*} z\right) = \frac{1}{2\pi \mathrm{i}^\nu} \int_{-\pi}^{\pi} \exp\left\{\mathrm{i}\nu\left(\frac{z}{z^*}\cos u + u\right)\right\} \mathrm{d}u, \tag{31}$$

which gives

$$I_{n_1,n_2} = \frac{1}{2\pi \mathrm{i}^\nu} \int_{z_h}^{1} \int_{-\pi}^{\pi} g(z) \exp\{\mathrm{i}\nu\Phi(u,z)\}\ \mathrm{d}u\mathrm{d}z, \tag{32}$$

where $g(z)$ is an amplitude function which is defined as

$$g(z) = -\frac{(1-\mathrm{i})G(k_b)B_1C_{D_1}c_1M_{r_1}^2\sin(\alpha_1+\alpha_2)M_{r_2}k_y}{4\pi r M_x\sigma_2^{0.5}\left(1+M_{r_2}\right)^{0.5}\left[\frac{\sigma_2 M_{r_2}}{(1+M_{r_2})}+\frac{k_x}{2}\right]^{0.5}}E^*\left(\frac{2}{\sqrt{\pi}}\left[\frac{\sigma_2 M_{r_2}}{(1+M_{r_2})}+\frac{k_x}{2}\right]^{0.5}\right), \tag{33}$$

and $\Phi(u,z)$ is a phase function which is defined as

$$\Phi(u,z) = \frac{z}{z^*}\cos u + u - \Gamma(z), \tag{34}$$

with

$$\Gamma(z) = \frac{1}{M_{r_2}}\left[\frac{M_x\cot\theta_e}{z^*}+M_{T_2}\right]\bar{s}_L + \frac{1}{M_{r_2}}\left[\frac{M_{T_2}z\cot\theta_e}{z^*}-\frac{M_x}{z}\right]\bar{l}_2$$
$$+\frac{n_1B_1}{\nu}\left[\frac{(M_{T_1}+M_{T_2})}{M_{r_2}}\bar{s}_L - \frac{1}{M_{r_2}}\left[\frac{M_x}{z}-z\frac{M_{T_1}M_{T_2}}{M_x}\right]\bar{l}_2 + \bar{g}\frac{M_{T_1}}{M_x}-\frac{M_{r_1}}{zM_x}\bar{l}_1\right]. \tag{35}$$

where $\bar{l}_1 = 2l_1/D$, $\bar{l}_2 = 2l_2/D$, $\bar{s}_L = 2s_L/D$, $s_L = (s_2 - c_2/2)$ and $\bar{g} = 2g/D$.

3.2 Asymptotic analysis and quiet rotor design

A number of authors including Chako (1965) and Cooke (1982) have considered evaluating double integrals of the form given by eq. (32) asymptotically for the case where $|\nu| \to \infty$. These studies all demonstrate that the *principle contributions* to I_{n_1,n_2} arise from small regions of the integrand around certain *critical points* which for the purposes of the problem considered here can be divided into two general types:

(a) Stationary points of the phase function which occur either within the 'source annulus' or on the bounding curve of the annulus.
(b) Points on the source annulus boundary where the tangential derivative of the phase function vanishes.

In the following sections expressions for the leading order terms in the asymptotic expansion of I_{n_1,n_2} will be presented. It will be assumed that $B_1 \to \infty, B_2 \to \infty$ and that linear combinations of B_1 and B_2 can also be regarded as being infinitely large (i.e. $|\nu| \to \infty$, $|\omega| \to \infty$). One final assumption which will be made is that the absolute value of a ratio of large parameters can be regarded as being $O(1)$. Note that these assumptions will not hold valid for all possible tones and observer angles produced by the open rotors considered later. This work will require the partial derivatives of the phase function which are listed below as

$$\Phi_{1,0} = 1-\frac{z}{z^*}\sin u,\ \Phi_{0,1} = \frac{\cos u}{z^*} - \Gamma'(z),\ \Phi_{2,0} = -\frac{z}{z^*}\cos u,\quad \Phi_{1,1} = -\frac{\sin u}{z^*},\ \Phi_{0,2} = -\Gamma''(z),$$
$$\Phi_{3,0} = \frac{z}{z^*}\sin u,\ \Phi_{1,2} = 0,\ \Phi_{2,1} = -\frac{\cos u}{z^*},\ \Phi_{0,3} = -\Gamma'''(z). \tag{36}$$

Note that we have adopted the notation

$$\Phi_{p,q}(u,z) = \frac{\partial^{p+q}}{\partial u^p \partial z^q}\Phi(u,z). \tag{37}$$

We consider first the case of stationary points which occur within the source annulus and, adopting the terminology of Chako (1965), will refer to these points as *interior stationary points*. It is assumed that each of these interior stationary points lie within the source annulus sufficiently far away from the inner and outer edge of the annulus and also separated from other critical points by a sufficient distance such that the principle contribution to I_{n_1,n_2} from each point can be considered in isolation.

An interior stationary point occurs at $\{u,z\} = \{\tilde{u},\tilde{z}\}$ when $\Phi_{1,0} = \Phi_{0,1} = 0$. For now it will also be assumed that $\Phi_{2,0}\Phi_{0,2} \neq \Phi_{1,1}^2$ at any of these points. From the definition of the partial derivatives we can determine the location of the stationary points to be the solution to the following two equations,

$$\sin\tilde{u} = \frac{z^*}{\tilde{z}},\ \cos\tilde{u} = \Gamma'(\tilde{z})z^*, \tag{38}$$

or, on eliminating $\tilde{u}$, when

$$\tilde{z}^2 = z^{*2}[[\tilde{z}\Gamma'(\tilde{z})]^2 + 1]. \tag{39}$$

We follow the method of Cooke (1982) to evaluate the contribution to I_{n_1,n_2} from an interior stationary point for $|\nu| \to \infty$ which gives the following expression

$$I_{n_1,n_2} \sim \frac{\tilde{g}_{0,0}}{|\nu|\left|\tilde{\Phi}_{2,0}\tilde{\Phi}_{0,2} - \tilde{\Phi}_{1,1}^2\right|^{\frac{1}{2}}} \exp\left\{\mathrm{i}\nu\left(\tilde{\Phi}_{00} - \frac{\pi}{2}\right) + \mathrm{i}\frac{\pi}{4}\mathrm{sgn}(\nu)\mathrm{sgn}\left(\tilde{\Phi}_{2,0}\right)\left[1 + \mathrm{sgn}\left(\tilde{\Phi}_{2,0}\tilde{\Phi}_{0,2} - \tilde{\Phi}_{1,1}^2\right)\right]\right\}. \tag{40}$$

where the tilde on a parameter indicates that it is evaluated at the critical point.

If no stationary points exist within the domain of integration then the main contribution to I_{n_1,n_2} come from what Chako (1965) refers to as boundary critical points. Boundary critical points are those points on the boundary of the domain of integration at which the tangential derivative of Φ vanishes. In the case considered here, the domain is the annular region described by the radial coordinate z and the angle u. The tangential derivative of Φ vanishes, therefore, when $\Phi_u = 0$ and $z = 1$ or $z = z_h$. We will consider the contributions from the tip ($z = 1$). The boundary critical points for this case arise at $\sin u = z^*$ producing two solutions at the tip $(\hat{z}, \hat{u}_\pm)$

$$\hat{z} = 1,\ \hat{u}_\pm = \begin{cases} \sin^{-1}(z^*) \\ \pi\mathrm{sgn}(z^*) - \sin^{-1}(z^*)\,. \end{cases} \tag{41}$$

Following the method presented in Cooke (1982) we find that the two contributions $I^{\pm}_{n_1,n_2}$ from the tip to I_{n_1,n_2} are, to leading order, given by

$$I^{\pm}_{n_1,n_2} \sim \frac{\hat{g}_{0,0}\exp\left\{\mathrm{i}\nu\hat{\Phi}_{0,0} + \mathrm{i}\frac{\pi}{4}\mathrm{sgn}(\nu)\mathrm{sgn}\left(\hat{\Phi}_{2,0}\right)\right\}}{\mathrm{i}^{\nu+1}\sqrt{2\pi}\nu|\nu|^{1/2}\left|\hat{\Phi}_{2,0}\right|^{1/2}\hat{\Phi}_{0,1}}, \tag{42}$$

where the hat on a parameter indicates that it is evaluated at the critical point. Contributions from the hub region can be evaluated using the same method which yields a similar expression.

A plot of the sound pressure level spectrum calculated using the expressions given above for a straight-bladed rotor is shown in figure 10 below. Results calculated using a full numerical calculation of I_{n_1,n_2} (circles) are plotted along with the levels calculated using the asymptotic expressions derived in this paper (dots). There is generally reasonable agreement between the exact and asymptotic results which gives confidence in the accuracy (and usefulness) of the asymptotic expressions. The other point of note with these results is that tones associated with interior critical points (blue) are generally of a much higher level than tones associated with boundary critical points (red). Based on these results, one approach to reduce the overall level of noise produced by this noise source would be to design a rotor for which no interior critical points occur for all significant tones at important observer positions.

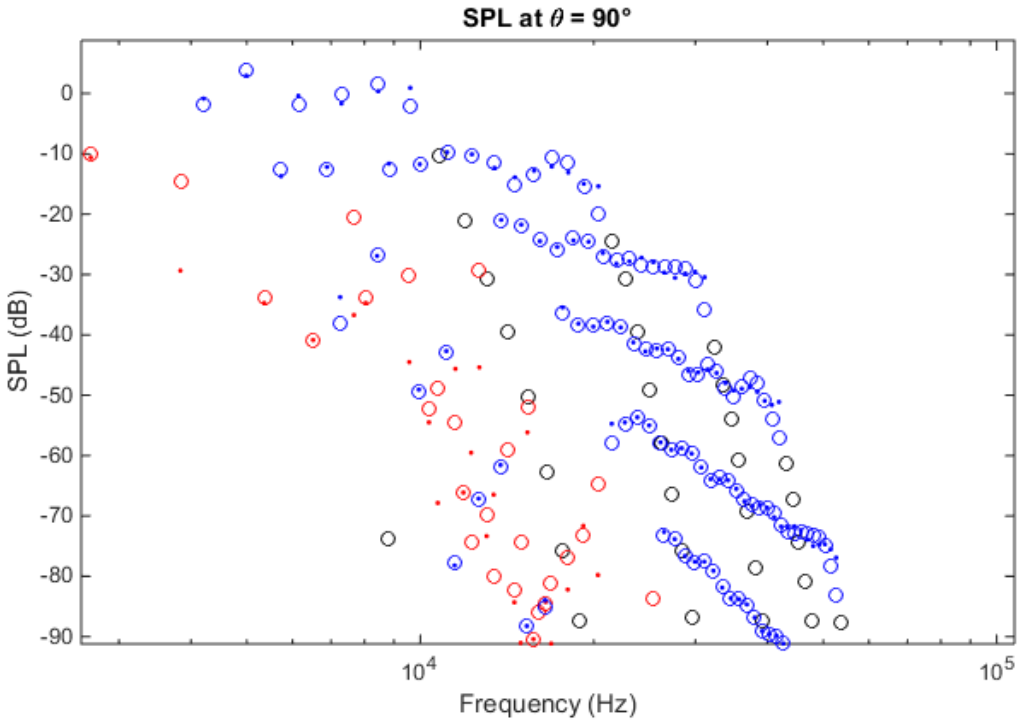

Figure 10: Plot of SPL vs frequency. Circles denote a numerical solution and dots denote an asymptotic solution. Normal interior critical point (blue), boundary critical point (red), $|z^*| > 1$ (black).

Recall that for $|z^*| > 0$, interior critical points are located at

$$\tilde{z}^2 = z^{*2}[[\tilde{z}\Gamma'(\tilde{z})]^2 + 1]. \tag{43}$$

For no lean and $|z^*| > 0$ we have $\Gamma(z)$ defined as

$$\Gamma(z) = \frac{1}{z^* \sin\theta_e}\frac{\bar{s}_L}{M_{r_2}} + \frac{n_1 B_1}{\nu}\bar{g}\frac{M_{T_1}}{M_x}. \tag{44}$$

It will also be useful to define $\Theta(z) = \bar{s}_L/M_{r_2}\sin\theta_e$ such that

$$\Gamma'(z) = \frac{1}{z^*}\Theta'(z). \tag{45}$$

Substituting into about eq. yields the following expression for ϕ for a 'critical design'

$$\Theta'(z) = \sqrt{1 - \left(\frac{z^*}{z}\right)^2}, \; z \geq |z^*|. \tag{46}$$

Rotors which have $\Theta'(z)$ larger than the 'critical design' defined by the equations above will have no interior critical points. Such a design can be attained by selecting an appropriate profile for the downstream blade leading edge sweep, $\bar{s}_L$. Examination of the asymptotic expression for the boundary critical points reveals that increases in blade sweep past the critical design will result in reductions in the level of the radiated sound (via the $\widehat{\Phi}_{0,1}$ term). Also note that increasing the sweep of the downstream blade row has the added effect of increasing the spacing between the two rotors which increases the wake width at the downstream rotor and decreases the amplitude of certain high frequency tones (via reducing the magnitude of the $G(k_b)$ term).

Figure 11 below plots the sound pressure level of 4 individual tones against a 'sweep parameter' λ, which is defined such that the critical design corresponds to $\lambda = 1$. Values of λ less than one have interior critical points on the blade whilst values of λ greater than one do not have interior critical points on the blade. It is clearly observed that, as expected, further increases in blade sweep past the critical design reduce the level of these tones.

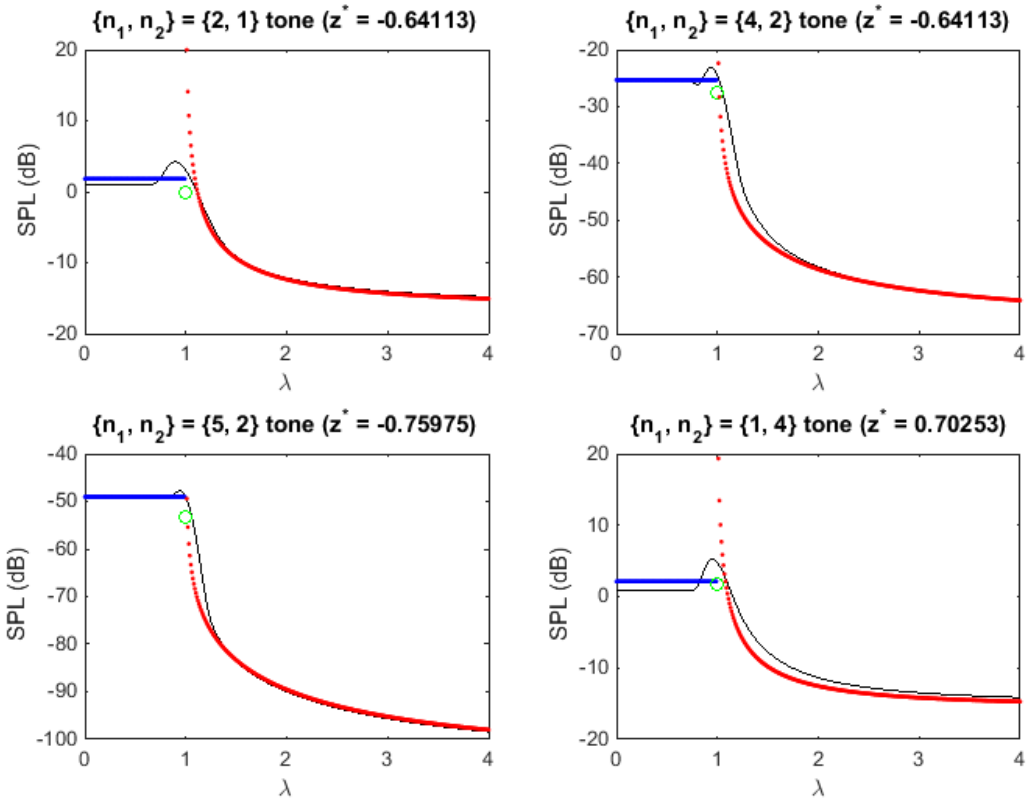

Figure 11: Plot of SPL versus 'sweep parameter', λ for 4 different tones. 'Exact' numerical solutions (black curve), Interior critical asymptotic solutions (blue dots), boundary critical asymptotic solutions (red dots), asymptotic solution for the critical design (green circle).

4. Conclusions

This paper has summarised a number of low- and high-speed experimental wind tunnel experiments undertaken using a model-scale open rotor test rig. Some of the issues encountered and the findings from these tests were described. A method was then presented for predicting the tonal noise produced by the interaction of the viscous wake from the upstream rotor with the downstream rotor. The paper concluded with an asymptotic analysis of the analytical equations which yielded insight into how the noise from this noise source could be reduced.

ACKNOWLEDGEMENTS

The author gratefully acknowledges the support of Rolls-Royce plc. during his time at the University Technology Centre in Gas Turbine Noise at the University of Southampton when much of this work was undertaken. He is indebted to collaborators at both Rolls-Royce and the University of Southampton who assisted with much of the work presented in this paper.

REFERENCES

Kingan, M.J., Ekoule, C.E., Parry, A.B., Britchford K., (2014) Analysis of Advanced Open Rotor Noise Measurements, Proceedings of the 19th AIAA/CEAS Aeroacoustics Conference, Atlanta, AIAA paper 2014-2745, 2014

Parker, R., Lathoud, M. (2010) Green Aeroengines: Technology to mitigate aviation impact on environment, Proceedings of the Institution of Mechanical Engineers, Part C: Journal of Mechanical Engineering Science March 1, 2010 vol. 224 no. 3 pp. 529-538

Parry, A. B. (1988) Theoretical prediction of counter-rotating propeller noise, PhD thesis, University of Leeds

Roger, M., Schram, C., Moreau, S. (2012) On vortex–airfoil interaction noise including span-end effects, with application to open-rotor aeroacoustics, Journal of Sound and Vibration, 333, pp. 283-306

Fuss, U. (2011) DREAM final workshop presentation, DREAM final workshop, September 20-22, 2011, Derby, United Kingdom.

Hanson, D. B. (1985) Noise of counter-rotation propellers, Journal of Aircraft, 1985, 22, pp. 609–17

Parry A., Kingan M.J., Tester B.J. Relative importance of open rotor tone and broadband noise sources, Proceedings of the 17th AIAA/CEAS Aeroacoustics Conference, Portland, AIAA Paper 2011-2763, 2011

T. J. Kirker, (1990) Procurement and Testing of a 1/5 Scale Advanced Counter Rotating Propfan Model, AIAA Paper 90-3975, 13th Aeroacoustics Conference, Tallahassee, FL, 22-24 Oct.

Paquet, C., Julliard, E., Genoulaz, N., Ricouard, J., and Spiegel, P. (2014). Z08: low-speed aero-acoustic experimental characterization of open rotor installation on aircraft. In 20th AIAA/CEAS Aeroacoustics Conference. AIAA Aviation.

Kingan, M. J. (2013) Open rotor broadband interaction noise, Journal of Sound and Vibration, vol. 332, pp. 3956-3970

Blandeau, V. P., Joseph. P. J., Kingan, M. J. Parry, A. B. (2013) Broadband noise predictions from uninstalled contra-rotating open rotors, International Journal of Aeroacoustics, vol. 12, pp. 245-282

Parry, A. B., Britchford, K. M., Kingan, M. J., Sureshkumar, P. (2012) Aeroacoustic tests of isolated open rotors at high speed, AIAA 2012-2220, 18th AIAA/CEAS Aeroacoustics conference, Colorado Springs, USA

Sureshkumar, P., Kingan, M. J., Parry, A. B. (2016) Predicting the noise of an open rotor in a wind tunnel, International Journal of Aeroacoustics (to appear).

Peake, N. and Boyd, W. (1993), 'Approximate Method for the Prediction of Propeller Noise Nearfield Effects', Journal of Aircraft 30(5).

van Oosten, N., Collin, D. (2014) NINHA: Noise Impact of aircraft with Novel engine configurations in mid- to High Altitude operations, Internoise Proceedings, Melbourne, Australia

Kingan, M. J. (2014) Advanced open rotor noise prediction, The Aeronautical Journal, vol. 118, issue 1208, pp. 1125-1135

Goldstein, M. E., (1976) Aeroacoustics, McGraw-Hill

Chako, N., (1965) Asymptotic expansions of double and multiple integrals occurring in diffraction theory, Journal of the Institute of Mathematics and its Applications, vol. 1, pp. 372-422

Cooke, J. C., (1982) Stationary phase in two dimensions, IMA Journal of Applied Mathematics, vol. 29, pp. 25-37